Low-energy neutral-current neutrino scattering on ^{128,130}Te isotopes

V. Tsakstara[*]
Division of Theoretical Physics, University of Ioannina, GR-45110 Ioannina, Greece

T. S. Kosmas[†,‡,§]
Institut für Kernphysik Technische Universität Darmstadt, D-64289 Darmstadt, Germany and
GSI, Theoretical Physics Division, D-64291 Darmstadt, Germany
(Received 18 March 2011; published 20 May 2011)

Differential, total, and cumulative cross section calculations for neutral current neutrino scattering on ^{128,130}Te isotopes are performed in the context of the quasiparticle random phase approximation by utilizing realistic two-nucleon forces. These isotopes are the main contents of detectors of ongoing experiments with multiple neutrino physics goals (COBRA and CUORE at Gran Sasso), including potential low-energy astrophysical neutrino (solar, supernova, geoneutrinos) detection. The incoming neutrino energy range adopted in our calculations ($\varepsilon_\nu \leqslant 100$ MeV) covers the low-energy β-beam neutrinos and the pion-muon stopped neutrino beams existing or planned to be conducted at future neutron spallation sources. The aim of these facilities is to measure neutrino-nucleus cross sections at low and intermediate neutrino energies with the hope of shedding light on open problems in neutrino-induced reactions on nuclei and neutrino astrophysics. Such probes motivate theoretical studies on weak responses of various nuclear systems; thus the evaluated cross sections may be useful in this direction.

DOI: 10.1103/PhysRevC.83.054612 PACS number(s): 25.30.Pt, 21.60.−n, 23.40.Bw, 24.10.−i

I. INTRODUCTION

In the past few decades, the search for semileptonic weak processes involving lepton-nucleus interactions (neutrino-induced reactions on nuclei, β-decay modes, nuclear muon capture, etc.) [1,2] has deepened our understanding of the fundamental electroweak interactions [3–5] and enriched our knowledge of nuclear structure [6–8] and nuclear astrophysics [9,10]. Such precious information inspired significant probes within and beyond the standard electroweak theory [4,5] and offered valuable interpretations to experiments searching for neutrino detection and neutrino intrinsic properties (neutrino masses, neutrino oscillations, etc.) [11–14]. Using nuclei as microlaboratories in reactor, accelerator, and underground neutrino production or detection experiments, neutrinos have been extensively investigated as key elementary particles in nuclear weak responses and in new astroparticle physics [4,5,9,10].

Furthermore, terrestrial neutrino telescopes have provided crucial information about the weak processes taking place in the interior of distant stars [15,16], as neutrinos are extremely sensitive signals for studying stellar evolution and astronuclear processes [9,10]. Thus, measurements of solar neutrinos (KAMLAND, Borexino, SNO experiments) have been used to test the standard solar model (for a recent review of this topic see, e.g., [13] and references therein), while in the near future probes with multiple neutrino physics goals (including low-energy astrophysical neutrinos and double-β-decay searches like the SNO+, MOON, and other experiments) [4,17–20] will be able to study low-energy solar neutrinos and geoneutrinos as well as conduct supernova searches. On the other hand, stellar evolution models developed recently to describe the explosion mechanism of type II supernovae have provided us with important information regarding the role of neutrinos in the evolution of massive stars, explosive nucleosynthesis, etc. [9,10,15,16]. However, uncertainties on astrophysical interactions of neutrinos and supernova physics opened many questions that are still unanswered, mostly due to our limited understanding and lack of measurements of neutrino-nucleus reaction cross sections [4,15,18,19]. In neutral current (NC) neutrino-nucleus interactions, which we address here, for example, there are little data for nuclear transitions induced by these neutrino processes [3,9,21].

Nowadays, there are two new possibilities of measuring neutrino-nucleus cross sections. The first is to use boosted β-decay radioactive nuclei as sources to produce neutrino beams of low and intermediate energies (β-beam neutrinos) [22–24]. The neutrino beam of such a facility is intense, collimated, and pure, appropriate for searching neutrino-nucleus interactions, and useful for the interpretation of low-energy neutrino signals [24,25]. For example, the analysis of supernova neutrino energy spectra, whenever observed, could be realized through proper measurements on low-energy β-beam spectra originating from boosted radioactive ions like ^{6}He, ^{18}Ne, and others [23–25]. The second possibility of measuring neutrino-nucleus cross sections is at stopped pion-muon neutrino facilities, existing (BooNe experiment, etc.) [26] or expected to be built near spallation neutron sources (ORLaND experiment, European Spallation Source) [27–29] (see also Ref. [15]). There, the neutrino beams may be intense neutrino pulses of energy spectra that could be unique for terrestrial studies of distant supernova reactions and also suitable for investigation of other neutrino-mediated processes, like solar reactions, etc. [14,15].

[*]vtsaksta@cc.uoi.gr
[†]Permanent address: Department of Physics, University of Ioannina, GR-45110 Ioannina, Greece.
[‡]hkosmas@uoi.gr
[§]t.kosmas@gsi.de

 ©2011 American Physical Society

Hence, the physics research that could be undertaken with the aforementioned neutrino-beam facilities is associated with the open questions in low- and intermediate-energy neutrinos in nuclear physics, particle physics, and astrophysics [14,23]. This research motivates a theoretical study of the advantages that carry various prominent nuclear regimes related to their use in neutrino experiments and to probe the structure of nucleons and nuclei [3,6]. It is worth mentioning that neutrinos excite nuclear modes (not accessible to electromagnetic probes) that allow us to study the characteristics of the nuclear dynamics and the nuclear weak responses that include polar-vector and axial-vector interactions [2,4,25].

From a nuclear theory point of view, the neutrino-nucleus cross section calculations at neutrino energies $\varepsilon_\nu \leqslant 100$ MeV (for neutral- and charged-current reactions) are, in addition, necessary in order to simulate the nuclear response to the energy spectra of various neutrino sources of promising detectors [4,18,20]. Such cross section calculations are useful in studies of solar, supernova neutrinos, and geoneutrinos, for exclusive, semi-inclusive (radiochemical), as well as inclusive processes [6,25] that provide us with significant information regarding the range of efficiency of several isotopes in low-energy neutrino searches [11–13].

Recently, as promising neutrino detectors based on neutrino-nucleus interactions have been considered, some materials used in double-β-decay searches like the molybdenum of the MOON experiment [4,19], the semiconductor detectors CdTe and CdZnTe of the COBRA experiment [17,18], etc. Also, the TeO_2 of the CUORE double-β-decay experiment is potentially a hybrid neutrino physics probe [20]. In the latter materials, the Te isotopes represent a large portion and an investigation of their potential use in low-energy neutrino detection (or neutrino cross section measurements) has not yet been addressed. It is the purpose of the present work to study the response of ^{128,130}Te isotopes (which have big abundances on the natural Te) to the low-energy neutrino spectra through detailed state-by-state cross section calculations of their neutral current reactions with neutrinos and antineutrinos.

The methods of state-by-state calculations need the explicit construction of all accessible final nuclear states in the context of a nuclear model, and they are reliably applicable to low and intermediate neutrino energies when the transitions to some definite nuclear states (ground state or some low-lying excitations) may dominate the cross section [3,6,30,31]. Such microscopic theoretical approaches used so far are mainly the shell model and the various versions of the random phase approximation (RPA) [3,30]. Recently [8], an advantageous numerical approach based on analytic evaluations of the reduced matrix elements of all basic tensor operators (produced by applying the Donnelly-Walecka projection method on the hadronic current density matrix elements) relevant to neutrino-nucleus processes [1,32–35] has been combined with a version of the quasiparticle RPA (QRPA) for state-by-state nuclear structure calculations. This method has been applied to neutral current neutrino-nucleus inelastic scattering [8,36], and it is adopted for the purposes of our present work.

We carry out extensive differential, total, and cumulative cross section calculations of (anti)neutrino scattering on ^{128,130}Te isotopes by employing the many-body nuclear wave functions produced within the $pp-nn$ quasiparticle random phase approximation (QRPA) that utilizes realistic two-nucleon forces [8,31,36]. Our attention is focused on inelastic scattering (the elastic channel is rather simple to calculate [11,12]) assuming that these nuclei, after their interaction with neutrinos, go to good quantum states of energies (E), angular momenta (J), parities (π), and other quantum numbers, so as the Donnelly-Walecka projection is applicable.

The rest of the article is organized as follows. At first (Sec. II), the main characteristics of the neutrino-nucleus interaction Hamiltonian are briefly summarized and a description of the cross section formalism based on the Donnelly-Walecka method and the numerical approach constructed in Ref. [8] is presented. Then (Sec. III), the main features of the QRPA are briefly outlined and the nuclear structure of the ^{128,130}Te isotopes is determined by adjusting appropriately the QRPA model parameters. The presented results of our cross section calculations for neutral-current neutrino and antineutrino scattering off the ^{128,130}Te isotopes are comprehensively discussed in Sec. IV. Finally (Sec. V), the main conclusions extracted from the present work are summarized.

II. BRIEF DESCRIPTION OF THE FORMALISM

In a terrestrial nuclear neutrino detector, but also in the stellar interior, the low-energy neutrinos ($\varepsilon_\nu \leqslant 100$ MeV) may interact with nuclei via neutral-current reactions described by

$$\nu_x(\tilde{\nu}_x) + (A, Z) \rightarrow \nu_x(\tilde{\nu}_x) + (A, Z)^*, \tag{1}$$

where $x = e, \mu, \tau$. While ν_μ, $\tilde{\nu}_\mu$, ν_τ, $\tilde{\nu}_\tau$ could not participate in charged-current reactions (they do not have sufficient energies to produce the heavy leptons $\mu^\pm$ and $\tau^\pm$), the ν_e and $\tilde{\nu}_e$ neutrinos may also interact through charged-current reactions as

$$\nu_e(\tilde{\nu}_e) + (A, Z) \rightarrow e^-(e^+) + (A, Z \pm 1)^*. \tag{2}$$

This is why from a collapsing star ν_μ, $\tilde{\nu}_\mu$, ν_τ, and $\tilde{\nu}_\tau$ neutrinos are emitted with higher average energies than those of ν_e and $\tilde{\nu}_e$ [9,10]. On the other hand, due to the fact that ν_e interact with the neutron-rich matter of the stellar environment more than $\tilde{\nu}_e$, they have lower average energy compared to that of the $\tilde{\nu}_e$.

Neutrino interactions in nuclei, according to the standard model, are mediated by boson exchange (Z for the neutral- and $W^\pm$ for the charged-current reactions) between the neutrino (lepton sector, relevant to fundamental properties of neutrinos and weak interactions) and the nucleon (baryon sector which is relevant to the nuclear weak responses we are interested in, in the present work). In the incoming neutrino energy range considered in the present paper, the weak interaction neutrino-nucleus Hamiltonian $\hat{H}_I$ is written in the usual effective current-current form as [1,2]

$$\hat{H}_I = -\frac{G}{\sqrt{2}} \int d^3x j_\mu^{\text{lept}}(\mathbf{x}) \hat{\mathcal{J}}^\mu(\mathbf{x}) \tag{3}$$

($G = 1.1664 \times 10^{-5}\,\text{GeV}^{-2}$ is the weak coupling constant), where j_μ^{lept} and $\mathcal{J}^\mu$ denote the leptonic and hadronic currents,

respectively. According to V-A theory, the leptonic current takes the form

$$j_\mu = \bar{\psi}_{\nu_\ell}(x)\gamma_\mu(1-\gamma_5)\psi_{\nu_\ell}(x),$$

where ψ_{ν_ℓ} are the (anti)neutrino spinors.

From a nuclear physics point of view, the hadronic current of Eq. (3) is of primary interest. Focusing on neutral current processes, the structure of both polar-vector and axial-vector components (neglecting the pseudoscalar contributions) is expressed by

$$\mathcal{J}_\lambda = \overline{\psi}_N \left\{ F_1^Z \gamma_\lambda + F_2^Z \frac{i\sigma_{\lambda\nu}q^\nu}{2M} + F_A^Z \gamma_\lambda\gamma_5 \right\} \psi_N. \quad (4)$$

The superscript Z denotes Z-exchange processes, ψ_N represent the nucleon (proton or neutron) spinors with mass M, and γ_λ, γ_5, $\sigma_{\lambda\nu}$ are the known Dirac matrices.

In Eq. (4), F_i^Z, $i = 1, 2$ represent the weak nucleon form factors given in terms of the well-known charge and electromagnetic form factors for proton ($F_{1,2}^p$) and neutron ($F_{1,2}^n$) by the expression (CVC theory) [2]

$$F_{1,2}^{Z(p,n)} = \left(\tfrac{1}{2} - \sin^2\theta_W\right) F_{1,2}^{p,n}\tau_0 - \sin^2\theta_W F_{1,2}^{p,n} \quad (5)$$

(θ_W is the Weinberg angle, $\sin^2\theta_W = 0.2325$). In addition, F_A^Z stands for the neutral current axial-vector form factor,

$$F_A^Z = \tfrac{1}{2} F_A\left(q_\mu^2\right)\tau_0, \quad (6)$$

where $\tau_0 = +1$ (-1) for protons (neutrons). For $F_A(q_\mu^2)$ we employ the dipole ansatz (see, e.g., Refs. [37,38]) and use as static value $g_A = -1.258$ (in the present work, the quenching effect is not taken into consideration for the axial-vector coupling constant g_A). q^μ denotes the four-momentum transfer to the nucleus, $q^\mu = (q_0, \mathbf{q})$, for which, in our convention, we write $q_\mu^2 \equiv q^\mu q_\mu = q_0^2 - \mathbf{q}^2$.

In the considered processes, low-energy neutrinos (or antineutrinos) with initial four-momentum $k_i = (\varepsilon_i, \mathbf{k}_i)$ are inelastically scattered from Te isotopes. For the even-even ^{128,130}Te isotopes, the initial nuclear state ($|i\rangle \equiv |J_i^{\pi_i} M_i\rangle$) is the ground state, $|J_i^{\pi_i}\rangle = |0_{\rm gs}^+\rangle$. After the reaction, the nucleus is left in an excited state $|f\rangle \equiv |J_f^{\pi_f} M_f\rangle$ (M_f and M_i are the magnetic quantum numbers). Then, the double-differential cross section of the reactions (1) is written as [1,2]

$$\left.\frac{d^2\sigma_{i\to f}}{d\Omega d\omega}\right|_{\nu/\bar{\nu}} = (2\pi)^4 \varepsilon_f^2 \sum_{s_f, s_i, M_f, M_i} (2J_i+1)^{-1} |\langle f|\hat{H}_I|i\rangle|^2, \quad (7)$$

where ε_f ($\mathbf{k}_f$) represent the energy (momentum) of the outgoing lepton (for massless neutrinos $|\mathbf{k}_f| = \varepsilon_f$). We define the four-momentum q^μ as $q^\mu = (k_i - k_f)^\mu$.

After applying, as in the Donnelly-Walecka method [1,32,33], a multipole analysis on the weak hadronic current, the double-differential cross section of Eq. (7) reads

$$\frac{d^2\sigma_{i\to f}}{d\Omega d\omega}(\phi,\theta,\omega,\varepsilon_i)|_{\nu/\bar{\nu}} = \delta(E_f - E_i - \omega)\frac{2G^2\varepsilon_f^2\cos^2(\theta/2)}{\pi(2J_i+1)}[\mathcal{C}_V + \mathcal{C}_A \mp \mathcal{C}_{VA}]. \quad (8)$$

The δ-function on the right-hand side of this equation denotes the energy conservation, so as

$$\omega = E_f - E_i = \varepsilon_i - \varepsilon_f,$$

where ω is the excitation energy of the nucleus, E_i and E_f represent the energy of the initial (ground) and final states of the studied nucleus, respectively (we neglect the nuclear recoil in the present calculations). In Eq. (8), the $(-)$ sign corresponds to scattering of neutrinos and the $(+)$ to scattering of antineutrinos.

The term $\mathcal{C}_V$ ($\mathcal{C}_A$) in Eq. (8) is a summation over the contributions coming from the polar-vector (axial-vector) multipole operators as [1,32–34]

$$\begin{aligned}\mathcal{C}_{V(A)} = &\sum_{J=0}^{\infty} |\langle J_f\|\widehat{M}_J^{(5)}(q) + \frac{\omega}{q}\widehat{L}_J^{(5)}(q)\|J_i\rangle|^2 \\ &+ \sum_{J=1}^{\infty}\left(-\frac{q_\mu^2}{2q^2} + \tan^2\frac{\theta}{2}\right)\left[|\langle J_f\|\widehat{T}_J^{\rm mag(5)}(q)\|J_i\rangle|^2\right. \\ &\left. + |\langle J_f\|\widehat{T}_J^{\rm el(5)}(q)\|J_i\rangle|^2\right]. \quad (9)\end{aligned}$$

The definitions of the eight multipole operators $\widehat{M}_J^{(5)}$, $\widehat{L}_J^{(5)}$, $\widehat{T}_J^{\rm el(5)}$, and $\widehat{T}_J^{\rm mag(5)}$, where the superscript 5 refers to the axial-vector components of the hadronic current, are given in the Appendix [1,32,33].

The interference term $\mathcal{C}_{VA}$ in Eq. (8) contains the product of transverse polar-vector and transverse axial-vector matrix elements as

$$\begin{aligned}\mathcal{C}_{VA} = &\, 2\tan\frac{\theta}{2}\left(-\frac{q_\mu^2}{q^2} + \tan^2\frac{\theta}{2}\right)^{1/2} \\ &\times \sum_{J=1}^{\infty} {\rm Re}\langle J_f\|\widehat{T}_J^{\rm mag}(q)\|J_i\rangle\langle J_f\|\widehat{T}_J^{\rm el}(q)\|J_i\rangle^*. \quad (10)\end{aligned}$$

Obviously, for normal parity transitions, $\mathcal{C}_{VA}$ contains contributions of $\widehat{T}_J^{\rm el}$ and $\widehat{T}_J^{\rm mag5}$ operators while for abnormal parity ones it contains matrix elements of $\widehat{T}_J^{\rm mag}$ and $\widehat{T}_J^{\rm el5}$.

The reduced one-body matrix elements of the eight multipole operators entering Eqs. (9) and (10) are evaluated through the use of the analytic formulas derived in Ref. [8] (see the Appendix).

The magnitude of the three-momentum transfer $q \equiv |\mathbf{q}|$ and the square of the four-momentum transfer q_μ^2 entering Eqs. (4)–(10) are written in terms of the kinematical parameters (laboratory scattering angle θ and lepton energies ε_i and

$\varepsilon_f = \varepsilon_i - \omega$) as

$$q \equiv |\mathbf{q}| = [\omega^2 + 4\varepsilon_i(\varepsilon_i - \omega)\sin^2(\theta/2)]^{1/2}, \qquad q_\mu^2 \equiv q_\mu q^\mu = -4\varepsilon_i(\varepsilon_i - \omega)\sin^2(\theta/2). \tag{11}$$

In the rest of this paper, for the sake of convenience, we use the symbol ε_ν instead of ε_i for the incoming neutrino energy.

III. THE MAIN FEATURES OF THE QRPA METHOD

The second basic ingredient in our present study is the construction of the initial and final nuclear states, $|J_i\rangle \equiv |J_i^{\pi_i}\rangle$ and $|J_f\rangle \equiv |J_f^{\pi_f}\rangle$, entering the cross sections of Eqs. (8)–(10). We deduce them within the quasiparticle random phase approximation, the main features of which are briefly outlined below [31,39–42].

The nuclear ground state ($|J_i\rangle$) of each isotope is well described and rather readily constructed by solving the BCS equations using as single-particle energies those extracted from the effective field of a Coulomb-corrected Woods-Saxon potential plus the pairing interaction part of a one-meson exchange Bonn-C two-body potential. It has been shown that this potential, in medium heavy and heavy nuclei, yields a good description of the giant dipole and spin-dipole resonances that are expected to dominate the low-energy neutrino-nucleus scattering cross sections [21].

The excited states derived by our method are generic states of $1p-1h$ structure. For neutral current neutrino-nucleus reactions, the appropriate version of the QRPA is the $pp-nn$ type in which the required two quasifermion operators $A^\dagger$, A, are defined as [31,39,40]

$$A_\tau^\dagger(kl, JM) \equiv (1+\delta_{kl})^{-\frac{1}{2}}[a_{\tau k}^\dagger a_{\tau l}^\dagger]_M^J, \tag{12}$$

$$\tilde{A}_\tau(kl, JM) = (-1)^{J-M} A_\tau(kl, J-M), \tag{13}$$

where

$$[a_{\tau k}^\dagger a_{\tau l}^\dagger]_M^J = \sum_{m_k, m_l} \langle j_k m_k j_l m_l | JM\rangle a_{\tau k m_k}^\dagger a_{\tau l m_l}^\dagger. \tag{14}$$

$a^\dagger$ and a are the quasiparticle creation and destruction operators, respectively. The operators $A^\dagger$, $\tilde{A}$ obey the boson commutation relations in a correlated RPA ground state [43].

In the $pp-nn$ QRPA, the phonon operator $\hat{Q}_{J^\pi M}^{m\,\dagger}$ in the angular momentum coupled representation is written as

$$\hat{Q}_{J^\pi M}^{m\dagger} = \sum_{\substack{k\le l \\ \tau}} \left[X_\tau^m(kl, J)A_\tau^\dagger(kl, JM) + Y_\tau^m(kl, J)\tilde{A}_\tau(kl, JM)\right] \tag{15}$$

(the indices k, l run over all single-particle levels of the chosen model space and τ is an isospin index for proton or neutron). Thus, in the QRPA the mth excited state of the multipolarity J^π, which is denoted as $|J_m^\pi M\rangle$, is derived by acting with the phonon operator of Eq. (15) on the QRPA vacuum $|\tilde{0}\rangle_{\mathrm{QRPA}}$ as [31,40]

$$\left|J_m^\pi M\right\rangle = \hat{Q}_{J^\pi M}^{m\dagger}|\tilde{0}\rangle_{\mathrm{QRPA}}. \tag{16}$$

The excitation spectrum of the studied nucleus is calculated by solving the eigenvalue problem (the $pp-nn$ QRPA equations), described by

$$\begin{pmatrix} \mathcal{A} & \mathcal{B} \\ -\mathcal{B} & -\mathcal{A} \end{pmatrix} \begin{pmatrix} X^m \\ Y^m \end{pmatrix} = \Omega_{J^\pi}^m \begin{pmatrix} X^m \\ Y^m \end{pmatrix}, \tag{17}$$

where $\Omega_{J^\pi}^m$ is the excitation energy of the state $|J_m^\pi\rangle$. The QRPA vectors X and Y, i.e., the forward- and backward-going amplitudes, respectively, are calculated separately for each multipole set of states of the nucleus in question.

The QRPA matrices $\mathcal{A}$ and $\mathcal{B}$ are derived by the RPA ground-state matrix elements of the double commutator of the nuclear Hamiltonian $\hat{H}$ with the operators of Eqs. (12) and (13) [31,41–43]. The operator $\hat{H}$, in addition to the kinetic energy and the effective field (a Woods-Saxon potential), contains the residual interaction (Bonn-C one-boson exchange potential) parametrized as we discuss below.

In the present study we assume that the QRPA excitations $|J_m^\pi\rangle$, having good angular momentum, parity, and energy, are induced in the nuclear target (detector) through its interaction with the incoming (anti)neutrino.

A. Determination of the QRPA parameters

As it is well known, the bare nucleon-nucleon residual interaction of the Bonn-C potential used in structure calculations referred to an isotope (A, Z) is initially constructed for all nuclear systems of mass number A (in our case the output of the extracted matrix elements is stored in two submatrices corresponding to the values of the two-nucleon isospin, $T = 0$ and $T = 1$), after choosing an active model space (we employ the same model space for proton and neutron configurations). The above matrix elements are subsequently adjusted to the specific isotope, (A, Z), through the use of four important parameters that renormalize the bare residual interaction, as follows [39–41].

At the BCS level, the pairing part of the bare residual interaction is multiplied by a factor g_{pair}^p for protons and g_{pair}^n for neutrons, and the magnitudes of these factors are separately adjusted, such as the empirical pairing gaps for protons and neutrons are correctly reproduced. The required empirical energy gaps are obtained through the separation energies S_p and S_n using appropriate semiempirical formulas [43]. At this stage, the probabilities for the single-particle levels being occupied or unoccupied are also determined through the well-known $V_{p(n)}$ and $U_{p(n)}$ amplitudes, respectively. This is a standard procedure and it is well known that within the BCS method the strength of the pairing interaction depends weakly on the size of the single-particle basis (when the basis is changed, the interaction is slightly modified as well) [41].

After settling the values of the pairing parameters, two other parameters are left to fix the scale of the particle-hole channel, g_{ph}, and the particle-particle channel, g_{pp}, of the bare residual interaction. In our method, this is done separately for each multipolarity J^π [31,39], in such a way that the low-lying QRPA excitations fit the experimental spectrum of the isotope in question (see concrete examples below).

B. The structure of the ^{128,130}Te isotopes

In this paper we perform explicit state-by-state calculations for the cross sections of (anti)neutrino scattering off the ^{128}Te

TABLE I. Parameters determining the pairing interaction for protons, $g^{p}_{\rm pair}$, and neutrons $g^{n}_{\rm pair}$. They reproduce rather well the corresponding (for each isotope) empirical energy gaps $\Delta^{\rm exp}_{p,n}$ listed also in this table (the values of the harmonic oscillator size parameter b used for ^{128,130}Te isotopes are also shown).

Nucleus	b (fm)	$g^{n}_{\rm pair}$	$g^{p}_{\rm pair}$	S_n	S_p	$\Delta^{\rm exp}_{p}$	$\Delta^{\rm th}_{p}$	$\Delta^{\rm exp}_{n}$	$\Delta^{\rm th}_{n}$
^{128}Te	2.252	1.088	0.875	8.775	9.574	1.093	1.103	1.294	1.293
^{130}Te	2.257	1.067	0.832	1.772	1.282	1.017	0.997	1.206	1.207

and ^{130}Te isotopes described by the reactions

$$^{128,130}\mathrm{Te}(\nu,\nu')^{128,130}\mathrm{Te}^{*} \tag{18}$$

and

$$^{128,130}\mathrm{Te}(\widetilde{\nu},\widetilde{\nu}')^{128,130}\mathrm{Te}^{*}\,. \tag{19}$$

Within the context of the $pp-nn$ type QRPA, the excited states of ^{128}Te* and ^{130}Te* isotopes, assuming spherically symmetric nuclei, are determined by adopting as active valence space for protons and neutrons the fifteen single-particle levels: $1p-0f-2s-1d-0g-2p-1f-0h$, where for each shell both the $\ell+1/2$ and $\ell-1/2$ subshells are included.

The ground states $|J^{\pi}\rangle=|0^{+}\rangle$ of the ^{128,130}Te isotopes are adjusted (by solving iteratively the BCS equations) with the values of the pairing-strength parameters listed in Table I. These parameters reproduce well the corresponding energy gaps, $\Delta^{\rm exp}_{p,n}$ for protons and neutrons, respectively, as it is shown in this table.

Next, the low-energy excitations of the ^{128}Te* and ^{130}Te* nuclei are fixed with the aid of the other two renormalization parameters (different for each multipolarity): $g_{\rm ph}$ for the particle-hole and $g_{\rm pp}$ for the particle-particle channel of the residual interaction. More specifically, the particle-hole interaction block is renormalized by the strength parameter $g_{\rm ph}$, which is adjusted by requiring the energy of the first excited state of each multipolarity to be correctly reproduced (this is almost independent of the size of the single-particle basis) [41].

The spectrum is, in general, not sensitive to the last parameter $g_{\rm pp}$, which tunes the second excited state of each multipolarity J^{π}. The obtained values for the parameters $g_{\rm ph}$ and $g_{\rm pp}$, in the case of ^{128}Te, with the exceptions of the 0^{+} multipolarity (for which $g_{\rm ph}=0.37$ and $g_{\rm pp}=0.46$) and the 1^{-} multipolarity (for which $g_{\rm ph}=0.53$ and $g_{\rm pp}=1.00$), lie in the range $0.75\preceq g_{\rm ph}\preceq 1.15$ and $0.90\preceq g_{\rm pp}\preceq 1.20$. For the values of the parameters $g_{\rm ph}$ and $g_{\rm pp}$ in the case of the ^{130}Te isotope, it holds about the same situation.

IV. RESULTS AND DISCUSSION

A. Original results for $d^2\sigma/d\theta d\omega$

In the first step of the calculational procedure, we obtained original results for the double-differential cross section $d^2\sigma/d\Omega d\omega$ of Eq. (8) in both nuclear isotopes, ^{128,130}Te. From the variation of $d^2\sigma/d\theta d\omega(\theta,\omega,\varepsilon_\nu=\text{const})$ as a function of the excitation energy ω of the studied nucleus and the scattering angle θ of the outgoing lepton (for a fixed incoming neutrino energy $\varepsilon_\nu=$ const), we found that its angular variation is rather smooth while there are some pronounced peaks, mainly related to the dependence on ω. In addition, the cross sections are clearly backward peaked ($\theta\approx\pi$), a result that comes from the contribution of the transverse terms of Eq. (9).

Three-dimensional plots (surfaces) obtained from the results of our method for $d^2\sigma/d\theta d\omega(\theta,\omega,\varepsilon_\nu=\text{const})$ are similar to those of Ref. [44]. For comparison the reader is referred to Ref. [45,46], where the leading contribution of the $J^{\pi}=2^{+}$ multipolarity (in the case of the ^{64}Zn isotope) is illustrated.

B. The dependence of $d\sigma/d\omega$ on the excitation energy ω

In the second step of our calculations, we examine the behavior of the single-differential cross section $d\sigma/d\omega(\omega,\varepsilon_\nu)$ for various leading sets of multipole states (up to $J^{\pi}=6^{\pm}$) in the incoming neutrino energy range $0\leqslant\varepsilon_\nu\leqslant$ 100 MeV.

The results of such original state-by-state QRPA calculations for the most important multipolarities, which are the low spin-J ones, for the positive parity transitions $(0^{+},1^{+},2^{+})$ are illustrated in Fig. 1 (upper panel), and for the negative parity transitions $(1^{-},2^{-},3^{-})$ in Fig. 1 (lower panel). In this figure the cross sections refer to a typical rather high incoming neutrino energy, $\varepsilon_\nu=60$ MeV, but such plots could be also made for other values of ε_ν (see below).

As it is generally expected for inelastic scattering of low-energy neutrinos and antineutrinos from medium and heavy nuclei, the leading multipoles, which yield the most important cross sections, are the $J^{\pi}=1^{+}$ and $J^{\pi}=1^{-}$ multipoles. The maximum peak appears in the case of the 1^{+} multipole, in which the axial-vector pieces L^{5}_{1} and $\mathrm{T}^{\rm el5}_{1}$ (they are of order unity) dominate over the vector piece $\mathrm{T}^{\rm mag}_{1}$ (this is of order q/M) [2]. Since q is rather small in the case of low-energy neutrino scattering studied here, the axial-vector matrix elements dominate over the vector ones (even by an order of magnitude or more).

Our code initially gives original results for $d\sigma/d\omega(\omega,\varepsilon_\nu)$ separately for each multipolarity (in ascending order with respect to the QRPA excitation energy of each multipolarity). The obtained cross sections refer to all multipolarities up to $J^{\pi}\leqslant 8^{\pm}$ and incoming neutrino energies $0\leqslant\varepsilon_\nu\leqslant$ 100 MeV with an energy step $\Delta\varepsilon_\nu=1$ MeV. In order to study the dependence of $d\sigma/d\omega$ on the excitation energy ω throughout the entire QRPA spectrum of the isotope in question, a rearrangement of all excitations ω (974 states with $J^{\pi}\leqslant 8^{\pm}$) in ascending order, with the corresponding cross sections $d\sigma/d\omega$, is required. This was performed by using a special code (SORTMATR, appropriate for matrices). The variation of $d\sigma/d\omega(\omega,\varepsilon_\nu=\text{const})$ in the case of the

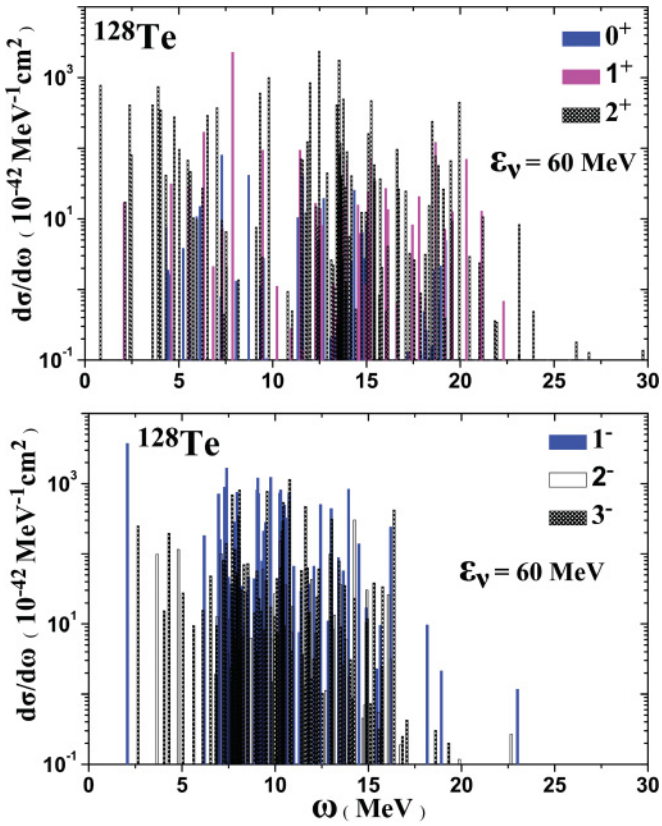

FIG. 1. (Color online) Differential cross section $d\sigma/d\omega$ as a function of the excitation energy ω of the nucleus ^{128}Te for the 0^+, 1^+, 2^+ (upper panel) and 1^-, 2^-, 3^- (lower panel) multipole states.

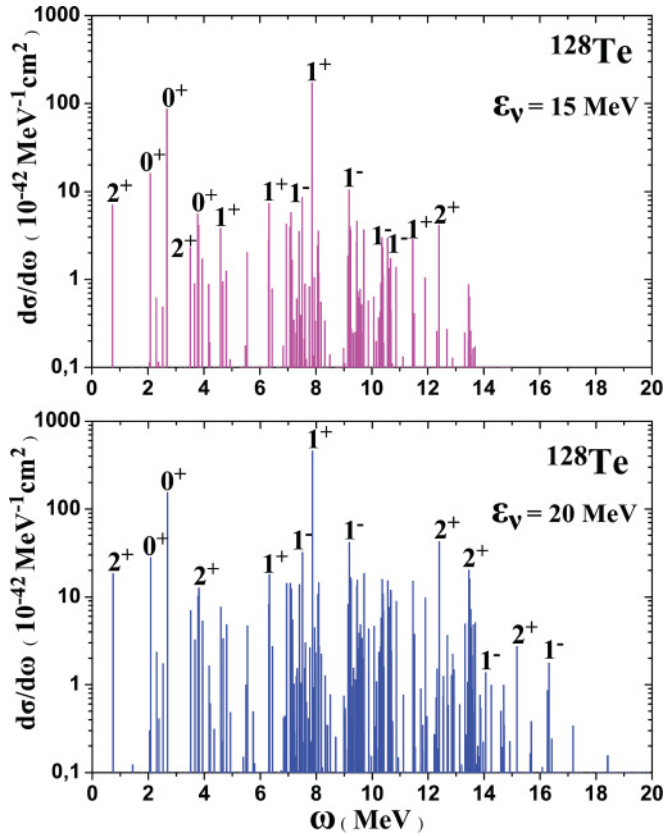

FIG. 2. (Color online) Differential cross section $d\sigma/d\omega(\omega)$ as a function of the excitation energy ω for the nucleus ^{128}Te. The incoming neutrino energy was $\varepsilon_\nu = 15$ MeV (upper panel) and $\varepsilon_\nu = 20$ MeV (lower panel).

reaction ^{128}Te$(\nu, \nu')^{128}$Te* is demonstrated in Fig. 2 and that in the case of ^{130}Te$(\nu, \nu')^{130}$Te* in Fig. 3. For both reactions, the $d\sigma/d\omega(\omega, \varepsilon_\nu = \text{const})$ presents some characteristic clearly pronounced peaks at various excitation energies ω (depending on ε_ν) and specifically for transitions $J^\pi = 1^+, 1^-$ but also for $J^\pi = 0^+, 2^+$.

We have chosen to show the dependence of $d\sigma/d\omega(\omega, \varepsilon_\nu = \text{const})$ for two values of incoming neutrino energy at $\varepsilon_\nu = 15$ MeV and $\varepsilon_\nu = 20$ MeV, i.e., a bit higher than the mean energies of supernova electron neutrinos, ν_e, and electron antineutrinos, $\widetilde{\nu}_e$, respectively [10]. We mention that in recent supernova neutrino simulations the mean energies $\langle \varepsilon_{\nu_e} \rangle = 11 - 12$ MeV, for ν_e, and $\langle \varepsilon_{\widetilde{\nu}_e} \rangle = 16 - 18$ MeV, for $\widetilde{\nu}_e$, have been chosen [4,10].

From this study we see that for ε_ν= 15 MeV, in the reaction ^{128}Te$(\nu, \nu')^{128}$Te* the maximum peak corresponds to a $J^\pi = 1^+$ transition (at $\omega = 7.867$ MeV) that is expected even in the long-wavelength limit [2]. The other peaks correspond to a 0^+ state with energy $\omega = 2.684$ MeV, to a 1^- state with energy $\omega = 9.182$ MeV, and to the first 2^+ state, 2_1^+ (and the first excitation above the ground state) with energy $\omega = 0.741$ MeV. For incoming neutrino energy $\varepsilon_\nu = 20$ MeV, the situation is clearly different only in the region $12 \leqslant \varepsilon_\nu \leqslant 18$ MeV.

From the corresponding investigation of $d\sigma/d\omega(\omega)$ in the reaction ^{130}Te$(\nu, \nu')^{130}$Te*, incoming neutrino energy $\varepsilon_\nu = 15$ MeV, we observed that the highest peaks correspond to two adjacent 1^+ transitions with energies $\omega = 7.572$ MeV and $\omega = 7.621$ MeV. The other principal peaks correspond to a 0^+ state with energy $\omega = 2.431$ MeV and to a 1^- state with energy $\omega = 9.719$ MeV. The dominance of the rest peaks is not very different than that of the isotope ^{128}Te (see Fig. 3).

The important implication of such a study for $d\sigma/d\omega(\omega, \varepsilon_\nu)$ is that the dominance of the peaks changes rather significantly with the incoming neutrino energy ε_ν, especially for higher energies, $\varepsilon_\nu = 40 - 60$ MeV. In more detail, for the reaction ^{128}Te$(\nu, \nu')^{128}$Te*, $\varepsilon_\nu = 50$ MeV, the maximum peak occurs for the $J^\pi = 1^+$ transition at $\omega = 7.867$ MeV, but the next peak corresponds to a 2^+ state with energy $\omega = 12.399$ MeV.

Regarding comparison with other methods, the most pronounced peaks in our calculations appear for $J^\pi = 1^+, 1^-$ at the region $\omega \approx 8 - 10$ MeV of the excitation spectrum. In continuum RPA (CRPA) calculations [44,47–50], even though in many of them transitions (from the ground state) to bound nucleon states are not included, it is interesting that the principal peaks found to lie in the energy region $\omega \approx 9 - 11$ MeV (see, e.g., for ^{208}Pb in Ref. [44,47]), i.e., in close agreement with our calculations.

Furthermore, the illustrated axial-vector dominance at rather low-energy excitations ($\omega \approx 10$ MeV) is expected (for heavy nuclei) due to the fact that the neutral current inelastic neutrino scattering is dominantly isovector in nature. This implies dominant excitations of isovector spin-flip transitions

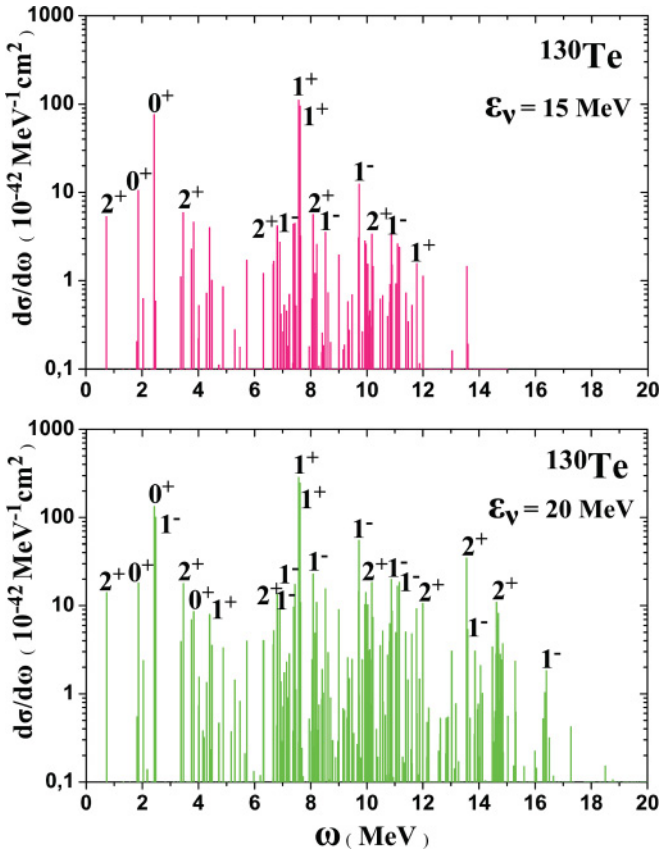

FIG. 3. (Color online) Same as in Fig. 2 but now for the ^{130}Te isotope.

of low-J multipolarities (isoscalar spin-flip excitations in inelastic neutrino scattering are of a few percent of the isovector ones) obtained in Figs. 1, 2, and 3 [21].

We note that due to their individual characteristics, the $J^\pi = 0^+$ and $J^\pi = 1^-$ excitations in the present calculations have been handled in a special way; we devote the subsections below to this description.

1. The $J = 0$ multipole contributions

As can be seen from Eq. (9), in the case of $|J^\pi\rangle = |0^+\rangle$ channel, only Coulomb and longitudinal terms of the polar vector current contribute and, in general, such transitions are expected to be suppressed (sometimes even by about an order of magnitude or more) [2]. However, for incoming neutrino energies $\varepsilon_\nu \lesssim 20$ MeV, in the case of Figs. 2 and 3, some 0^+ transitions are well pronounced and this can be explained as follows.

For the 0^+ transitions, the polar vector current operator is

$$M^0_0(q\mathbf{x}) = j_0(q\mathbf{x})Y^0_0 \;=\; j_0(q\mathbf{x})/\sqrt{4\pi}\,, \tag{20}$$

of which the matrix elements (as an energy-dependent operator) between the ground state, $|e_{\rm gs}\rangle = |0^+_1\rangle$, and any final $|J^\pi_m\rangle = |0^+_m\rangle$ state, are nonzero, i.e.,

$$\left\langle J^\pi_m \middle| M^0_0(q\mathbf{x})|e_{\rm gs}\right\rangle = \langle 0^+_m|M^0_0(q\mathbf{x})|0^+_1\rangle \neq 0\,. \tag{21}$$

In order to estimate the magnitude of these matrix elements, we discuss the special case of the long-wavelength limit, where the operator M^0_0 reduces to

$$M^0_0(q\mathbf{x}) \to (1/\sqrt{4\pi})[1 - (q/Q)^2(Qx)^2/6 + \cdots]. \tag{22}$$

Q, as usual, is chosen to be a value of momentum transfer to the nucleus such that $Q \approx R^{-1}$, where R denotes the nuclear radius. Then, for elastic scattering, for which $|0^+_m\rangle = |0^+_1\rangle$ in Eq. (21), the contribution comes from the operator

$$M^0_0(q\mathbf{x}) \to (1/\sqrt{4\pi}) \quad \text{(elastic)}\,, \tag{23}$$

which gives rise to the ground state to ground state (GS $\to$ GS) transitions (coherent channel). This multipole only enters in elastic scattering and it cannot, of course, produce inelastic transitions. Previous QRPA calculations have verified that the elastic channel is the dominant one for incoming neutrino energies (depending on the nuclear system) smaller than $\varepsilon_\nu \approx 50 - 70$ MeV [36].

For inelastic scattering, where the leading term in the low-q expansion vanishes (since $|0^+_m\rangle$ and $|0^+_1\rangle$ for $m \neq 1$ are orthogonal), the main contribution comes from the second term in Eq. (22), i.e.,

$$M^0_0(q\mathbf{x}) \to (q/Q)^2[(1/\sqrt{4\pi})(Qx)^2/6] \quad \text{(inelastic)}\,. \tag{24}$$

Hence, in this case, the low-q behavior of the inelastic Coulomb monopole is the same as for the Coulomb quadrapole, since both matrix elements are proportional to $(q/Q)^2$ [2,21]. As can be seen from Figs. 1 and 2, the 0^+ and 2^+ transitions have comparable contributions, but previous CRPA calculations have found, in general, a rather strong suppression of the 0^+ excitations [47,50].

In the case when $J^\pi = 0^-$ (only inelastic transitions occur), again only Coulomb and longitudinal terms contribute, but now of the axial-vector operators [see Eq. (9)]. For such transitions, the contributions come from the operators Σ''^0_0 and Ω^0_0 which are the only two multipole operators allowed (see the Appendix). However, these operators are not the dominant ones [2], and this is why the 0^- transitions are not included in the principal low-J contributions of Fig. 1. Such results, obtained with our QRPA method, have been published elsewhere [46,51].

2. The $J = 1^-$ multipole contributions

Special attention has been paid to the detailed study of the pronounced 1^- multipole contribution because, according to previous QRPA calculations of transition rates in semileptonic processes [52–54], they contain spurious admixtures originating from the center of mass motion. In more detail, the contaminations of the 1^- multipolarity are due to the use of non-self-consistent single-particle energies, which destroys the translational invariance of the nuclear Hamiltonian and inserts spurious excitations into the spectrum, as well as a truncated model space in the QRPA. For these reasons, the spurious center-of-mass state is not completely separated from the real nuclear excitations [52].

As it was found [52], the spurious admixtures inserted in the 1^- RPA excitation modes affect mostly the lowest-lying 1^-_1 state, a result that we adopt in the present work. In Ref. [52] an approximate method of removing the spurious 1^- components

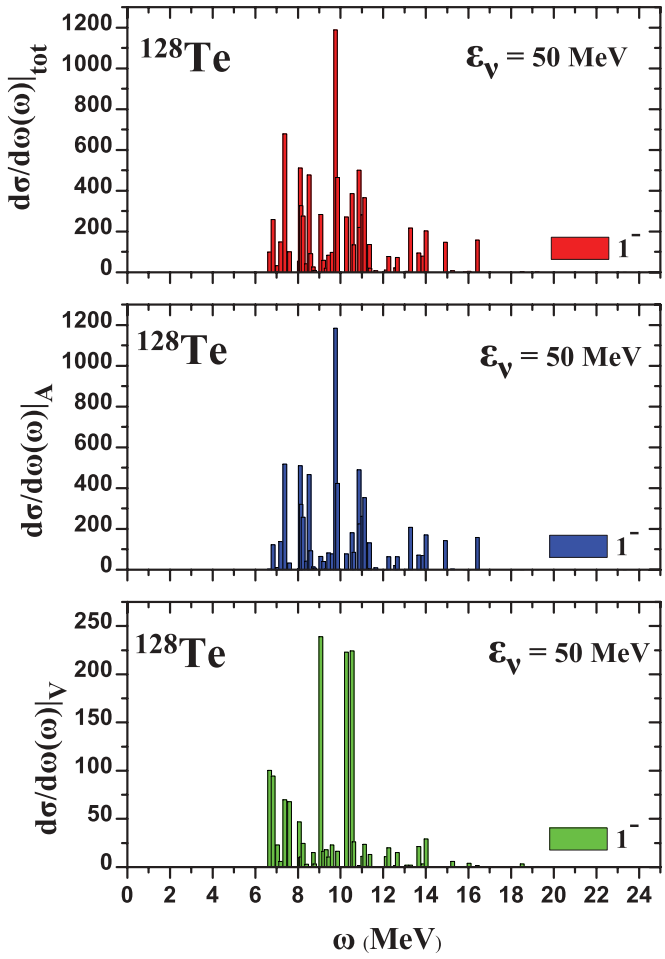

FIG. 4. (Color online) Individual contributions of polar-vector $\frac{d\sigma}{d\omega}|_V$ and axial-vector $\frac{d\sigma}{d\omega}|_A$ to the single-differential cross section $\frac{d\sigma}{d\omega}|_{\rm tot}$ of the 1^- multipolarity (in the ^{128}Te isotope) for incoming neutrino energy $\varepsilon_\nu = 50$ MeV (the differential cross sections are in units $\times 10^{-42}$ cm^2 MeV^{-1}).

was constructed based on the evaluation of the purely spurious state $|S\rangle$ and attached to the $pp - nn$ QRPA calculations.

In the present paper, in order to obtain realistic cross sections for the pronounced contribution of the 1^- channel, we worked out as in Ref. [52] and constructed the properly normalized purely spurious state $|S\rangle$ obtained from the center-of-mass operator **R**. We considered the first state of the 1^- multipolarity, 1^-_1, as fully spurious, and we treated the other states as the physical ones. In this way, we estimated a spuriousness of about 22.5% of the total strength of the 1^- multipolarity.

In Fig. 4 we plot the results obtained this way for the cross section $d\sigma/d\omega(\omega)$ of the 1^- multipolarity in ^{128}Te (incoming neutrino energy $\varepsilon_\nu = 50$ MeV). These results have been obtained by performing additional calculations for $d\sigma/d\omega$ in the case of the reaction (18) and using a different (larger) model space. In Fig. 4 we demonstrate separately the partial polar-vector and axial-vector contributions. As can be seen, the highest peaks of $d\sigma/d\omega(\omega)$ occur around $\omega \simeq 9 - 11$ MeV.

After removing the spurious 1^- contaminations, the individual axial-vector contributions $\frac{d\sigma}{d\omega}|_A$ are larger than the polar-vector $\frac{d\sigma}{d\omega}|_V$ ones by a factor of about 5. Hence, the total differential cross section, $\frac{d\sigma}{d\omega}|_{\rm tot}$, of the 1^- multipolarity (^{128}Te isotope for $\varepsilon_\nu = 50$ MeV) is about equal to the axial vector part. We mention that the difference between $\frac{d\sigma}{d\omega}|_{\rm tot}$ and the sum of axial vector $\frac{d\sigma}{d\omega}|_A$ and vector $\frac{d\sigma}{d\omega}|_V$ terms in Fig. 4 is due to the interference term $\frac{d\sigma}{d\omega}|_{VA}$, which is not shown in this figure (see discussion below). Concerning the corresponding hadronic current operators giving the results of Fig. 4 (middle and lower panels), we conclude that the normal parity axial vector component $T_1^{\rm mag5}$ dominates over the polar-vector ones M_1, L_1, and $T_1^{\rm el}$.

C. Antineutrino cross sections $d\sigma/d\omega(\omega, \varepsilon_\nu = \text{const})$

In Table II, we compare the cross sections $d\sigma/d\omega$ of each of the leading (low-J) multipolarities 0^-, 0^+, 1^-, 1^+, 2^-, 2^+, 3^-, and 3^+, in the neutrino reactions ^{128,130}Te$(\nu, \nu')^{128,130}$Te* and in the antineutrino reactions ^{128,130}Te$(\widetilde{\nu}, \widetilde{\nu}')^{128,130}$Te* (typical incoming neutrino energy $\varepsilon_\nu = 60$ MeV). The conclusion that comes out of the results of this table is that for normal parity transitions (0^+, 1^-, 2^+, 3^-), the cross sections of neutrinos are greater than those of antineutrino ones, while for abnormal parity transitions (0^-, 1^+, 2^-, 3^+), the cross sections of antineutrinos exceed those of neutrinos.

As a further investigation we examine the variation of the difference

$$\left.\frac{d\sigma}{d\omega}\right|_{\nu} - \left.\frac{d\sigma}{d\omega}\right|_{\widetilde{\nu}} = -2\left.\frac{d\sigma}{d\omega}\right|_{VA} \tag{25}$$

TABLE II. Comparison between the total contributions to $d\sigma/d\omega|_\nu$ and $d\sigma/d\omega|_{\widetilde{\nu}}$ of each of the multipolarities 0^-, 0^+, 1^-, 1^+, 2^-, 2^+, 3^-, and 3^+, for the reactions ^{128,130}Te$(\nu, \nu')^{128,130}$Te* and ^{128,130}Te$(\widetilde{\nu}, \widetilde{\nu}')^{128,130}$Te* ($\varepsilon_\nu = 60$ MeV).

		$d\sigma/d\omega(\times 10^{-40})$ cm^2 MeV^{-1} of Multipolarity							
	$\nu/\widetilde{\nu}$	0^-	0^+	1^-	1^+	2^-	2^+	3^-	3^+
^{128}Te	ν	12.72	26.53	157.47	32.69	14.81	143.01	87.24	3.34
	$\widetilde{\nu}$	12.72	26.53	146.32	38.04	19.37	138.35	84.76	4.36
^{130}Te	ν	8.48	35.84	210.71	31.85	14.37	142.28	90.26	3.35
	$\widetilde{\nu}$	8.48	35.84	191.94	37.13	18.19	138.10	87.83	4.38

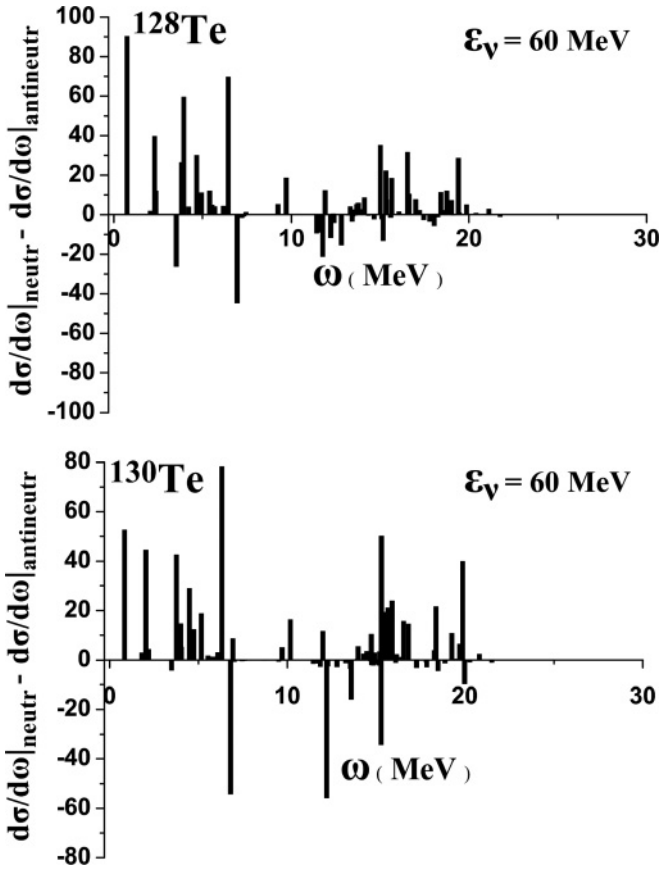

FIG. 5. The difference between $d\sigma/d\omega|_\nu$ of the reaction Te(ν, ν')Te* and $d\sigma/d\omega|_{\widetilde{\nu}}$ of the reaction Te$(\widetilde{\nu}, \widetilde{\nu}')$Te* for ^{128}Te (upper panel) and ^{130}Te (lower panel). These results refer to the dominant multipole states 2^+.

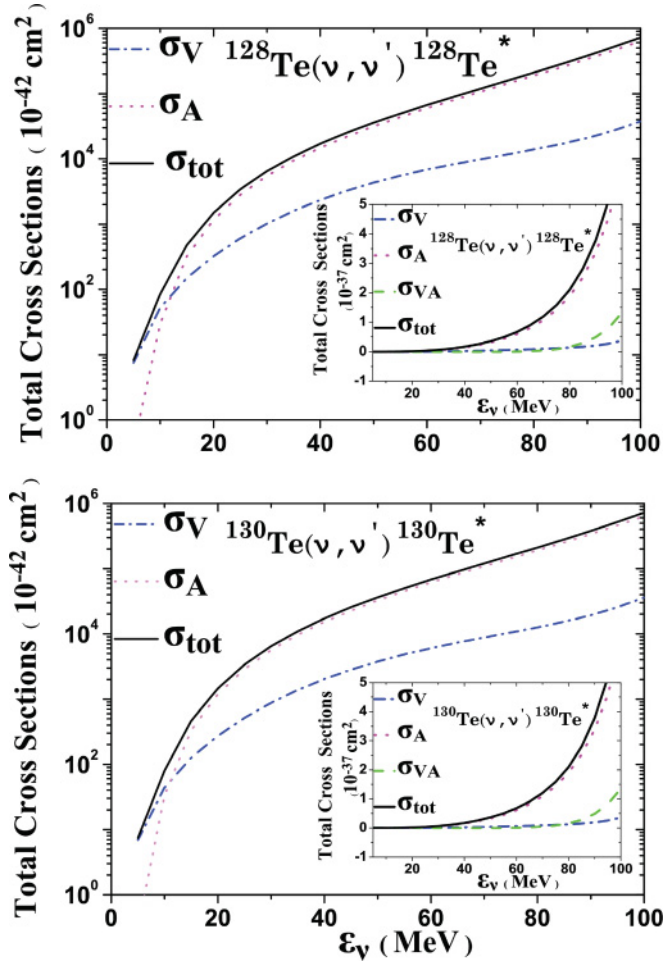

FIG. 6. (Color online) Total cross sections $\sigma_{\rm tot}$ for the reaction ^{128}Te$(\nu, \nu')^{128}$Te* (upper panel) and for ^{130}Te$(\nu, \nu')^{130}$Te* (lower panel). The individual contributions of the polar vector σ_V, the axial vector σ_A, and the interference term σ_{VA} (see the text) are also illustrated.

vs the excitation energy ω, which is twice the interference term of polar-vector and axial-vector contributions [see Eq. (10)]. In Fig. 5, we compare the $d\sigma/d\omega(\omega)$ of neutrino reactions, Eq. (18), with that of the antineutrino ones, Eq. (19) (the incoming neutrino energy is $\varepsilon_\nu = 60$ MeV), by plotting the difference defined in Eq. (25) in the case of the 2^+ transitions (upper panel for ^{128}Te and lower panel for ^{130}Te). The global view favors the neutrino cross sections, which are larger throughout the nuclear spectrum except for some individual (exclusive) transitions for which the antineutrino cross section is bigger. We note that we have paid special attention on the 2^+ multipolarity because most of the low-lying excitations of both ^{128,130}Te isotopes are 2^+ states [46,55].

D. Total cross sections

In the final step of our calculations we study total cross sections for the reactions Eqs. (18) and (19). In Fig. 6, we plot the total cross section $\sigma_{\rm tot}$ (in logarithmic and linear scale) of the reactions ^{128}Te$(\nu, \nu')^{128}$Te* (upper panel) and ^{130}Te$(\nu, \nu')^{130}$Te* (lower panel) as a function of the incoming neutrino energy ε_ν. For each reaction, the individual polar-vector, σ_V, and axial-vector, σ_A, parts as well as the interference term σ_{VA} are also illustrated. The latter individual cross sections have been obtained from the corresponding double-differential ones, $\mathcal{C}_V$, $\mathcal{C}_A$, and $\mathcal{C}_{VA}$ of Eqs. (9) and (10), respectively, by integrating over angles and summing over partial cross section throughout the excitation spectrum of the isotope in question. All calculations of the type $\sigma(\varepsilon_\nu)$ for $0 \leqslant \varepsilon_\nu \leqslant 100$ MeV have been performed with a step $\Delta\varepsilon_\nu = 1$ MeV.

By comparing similar graphs in the upper and lower panels, we see that there are qualitative and quantitative similarities of the cross sections for ^{128}Te and ^{130}Te in all plots of Fig. 6, except for a slight quantitative difference between the curves of the interference term σ_{VA}. We note that the latter curves are slightly negative in the energy region $25 \preceq \varepsilon_\nu \preceq 55$ MeV for both isotopes (log scale). For neutrino energies $\varepsilon_\nu \preceq 5 - 8$ MeV, the polar-vector contribution σ_V dominates, while for large energies the axial-vector cross section σ_A is approximately equal to the total cross section $\sigma_{\rm tot}$ [2,8].

As we have discussed in Sec. IV B, the polar-vector contribution is, in general, suppressed for large energies by more than one order of magnitude, which shows that the axial vector current is clearly more sensitive to the weak neutrino probes. As can be seen from Eqs. (4) and (6), the axial vector hadronic current is completely isovector, which means that

the isovector excitations dominate over the isoscalar ones. Furthermore, the isoscalar excitations are even suppressed due to the presence of the $\sin^2\theta_W$ in the form factors of Eq. (5), from where it becomes obvious that the isoscalar polar-vector form factors are considerably smaller than the isovector ones. In the proton-neutron representation we work here, this implies that the contribution of neutrons is significantly larger than that of the protons in all plots of Fig. 6 [56].

By summing the cross sections of Fig. 6 according to Eq. (8), we obtain the cross sections for antineutrino reactions, Eq. (19), for each isotope. By comparing them with $\sigma|_{\nu}^{\rm tot}$ of the neutrino reactions (in the energy region of our calculations), we obtain the relation $\sigma|_{\tilde{\nu}}^{\rm tot} \simeq 0.97 - 0.98\sigma|_{\nu}^{\rm tot}$, which means that the neutrino and antineutrino cross sections are slightly different.

1. Cumulative cross sections

In Fig. 7 we illustrate the total cumulative cross section $\sigma_{\rm cum}(\omega)$ as a function of the excitation energy ω for both isotopes ^{128}Te and ^{130}Te. This physical quantity shows how the total cross section is added up as soon as the transition channels to higher excitation energies ω become open. We have chosen two (constant) values of the incoming neutrino energy, $\varepsilon_\nu = 30$ MeV and $\varepsilon_\nu = 50$ MeV, in order to demonstrate the accumulation of $\sigma_{\rm cum}(\omega, \varepsilon_\nu = {\rm const})$ with increasing ω. As can be seen from this figure, for both energies ε_ν the cross sections in the two isotopes are comparable. However, the $\sigma_{\rm cum}(\omega)$ of ^{128}Te isotope, for $\omega \preceq 15$ MeV, is a bit larger than that of ^{130}Te, but for $\omega \succeq 15$ MeV the opposite occurs due to the fact that the dominant transitions of ^{128}Te lie at lower energies compared to those of ^{130}Te (roughly speaking, the spectrum of ^{130}Te appears slightly displaced toward higher energies compared to that of ^{128}Te isotope). The most abrupt increase (in both isotopes) is observed at $\omega \approx 15$ MeV (the giant resonance region), and this is more clear in the case of $\varepsilon_\nu = 50$ MeV.

In general, for both isotopes, the cumulative cross section $\sigma_{\rm cum}(\omega)$ for $\varepsilon_\nu = 50$ MeV is shifted by a factor of about 7 toward higher values compared to that for $\varepsilon_\nu = 30$ MeV.

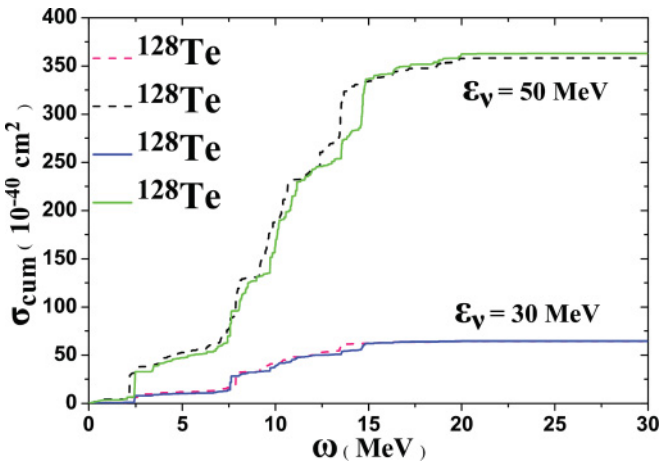

FIG. 7. (Color online) Cumulative cross sections $\sigma_{\rm cum}(\omega)$ for ^{128}Te and ^{130}Te for incoming neutrino energies $\varepsilon_\nu = 30, 50$ MeV.

E. Comparison with other methods

Regarding comparison of our method with other methods, to our knowledge there are no similar results to compare with our state-by-state (including transitions to bound states) cross section calculations on the ^{128,130}Te isotopes. The reliability of our method, however, comes out of the following comparisons: (i) for neutral current reactions, we compared point-by-point our QRPA results for the total cross section, $\sigma_{\rm tot}$, of the reaction ^{56}Fe$(\nu, \nu')^{56}$Fe* [36] with those of Ref. [48], which have been obtained by using the CRPA method, and (ii) for charged-current reactions (not addressed in the present work), we compared our QRPA cross sections for the reactions ^{56}Fe$(\nu, e^-)^{56}$Co* and ^{40}Ar$(\nu, e^-)^{40}$K* with those of Ref. [37,48,49]. In both cases the agreement is very good [36,57]. Even though the majority of available CRPA calculations do not include transitions to bound states, however, for heavy nuclear systems the most pronounced peaks of the original differential cross sections of the type $d\sigma/d\omega(\omega, \varepsilon_\nu = {\rm const})$ appear for low-spin transitions (from the ground state) in the energy region around $\omega = 9 - 11$ MeV [44]. These results are in good agreement with our present calculations (see Figs. 1–3).

We mention that results of state-by-state cross section calculations with our $pp - nn$ QRPA method, for the neutral current reactions ^{98}Mo$(\nu, \nu')^{98}$Mo* and ^{40}Ar$(\nu, \nu')^{40}$Ar*, have been published elsewhere [8,36]. The ^{98}Mo isotope constitutes one of the main materials of the detector of the MOON experiment at Japan [4,19].

Before closing, it is worth noting that the sensitivity of our results to modification of other parameters, like the axial vector coupling constant g_A, which describes the quenching effect [30], has not been tested in this work. We mention that in other electroweak processes (for which the matrix elements are not very sensitive to the nuclear structure) studied with the QRPA method, sometimes a rather strong quenching effect has been estimated. In Ref. [42], for example, by fitting simultaneously the QRPA particle-particle strength parameter, $g_{\rm pp}$, and the axial vector coupling constant, g_A, to three decay data (electron capture, single-β decay, and two-neutrino double-β decay) for the ^{128}Te isotope, the value $g_A \approx 0.4$ came out (see Ref. [42] and references therein). A comprehensive discussion of the quenching effect in studies of neutrino reactions with microscopic theories is done by Volpe *et al.* [30].

F. Connection with relevant experiments

As mentioned in the Introduction, the main goal of our present work was to study the neutrino ^{128,130}Te$(\nu, \nu')^{128,130}$Te* and antineutrino ^{128,130}Te$(\tilde{\nu}, \tilde{\nu}')^{128,130}$Te* reactions by carrying out extensive state-by-state calculations (with QRPA) and provide original results for various cross sections as the double-differential $d^2\sigma/d\Omega d\omega(\hat{\Omega}, \omega, \varepsilon_\nu)$, the single-differential $d\sigma/d\omega(\omega, \varepsilon_\nu)$, the total $\sigma_{\rm tot}(\varepsilon_\nu)$, and the cumulative $\sigma_{\rm cum}(\omega, \varepsilon_\nu = {\rm const})$. Behind the followed calculational procedure is hidden the assumption that the incoming neutrinos constitute a monoenergetic (monochromatic) beam of energy ε_ν.

The real neutrino sources, however, the astrophysical (solar, supernova, geoneutrinos) and the laboratory (β-beam, pion-muon stopped neutrino-beams, etc.), with few exceptions such as the ν_μ neutrino beam emerging from the π^+ decay at rest ($\varepsilon_\nu = 29.8$ MeV), the ^{7}Be solar neutrinos ($\varepsilon_\nu = 0.862$ MeV, according to the first direct sub-MeV solar neutrino rate measurement at Borexino [58]), etc., produce neutrinos that present a spectral distribution, characteristic of the source itself, and defined by

$$\frac{dN_\nu(\varepsilon_\nu)}{d\varepsilon_\nu} \equiv \eta(\varepsilon_\nu)\,. \tag{26}$$

N_ν denotes the number of neutrinos of the beam. Thus, for example, the ν_e neutrinos originating from pion-muon decay-at-rest have energy spectra approximately described by the well-known Michel distribution, while the supernova neutrinos are commonly interpreted by using for their energy spectra a two-parameter Fermi-Dirac or power law distributions [10]. The reader is referred, for the spectra η_{ν_e}, η_{ν_μ}, and $\eta_{\tilde{\nu}_\mu}$ and other experimental parameters of ongoing or past operating pion-muon stopped neutrino sources (MiniBooNE and BooNE, LAMPF, KARMEN, etc.), to the recent review of Ref. [26] and for the expected spectra at ORLaND experiment to Refs. [27,28,59].

For a connection of the present theoretical results with the neutrino experiments and the neutrino sources discussed in the Introduction, we have to carry out the folding (convolution) of the calculated cross sections with the distribution $\eta(\varepsilon_\nu)$ of the neutrino source of interest and estimate the response of ^{128,130}Te isotopes to the corresponding spectrum. For the differential $d\sigma/d\omega(\omega, \varepsilon_\nu)$ and total $\sigma_{\rm tot}(\varepsilon_\nu)$ cross sections, these responses (signals to the detector) are evaluated by

$$\left.\frac{d\sigma}{d\omega}\right|_{\rm sign}(\omega) = \int_\omega^\infty \frac{d\sigma}{d\omega}(\omega, \varepsilon_\nu)\eta(\varepsilon_\nu)d\varepsilon_\nu, \tag{27}$$

$$\sigma_{\rm sign}(\varepsilon_\nu) = \sigma_{\rm tot}(\varepsilon_\nu)\eta(\varepsilon_\nu). \tag{28}$$

In addition, by using $\sigma_{\rm tot}(\varepsilon_\nu)$, the flux averaged cross section $\langle\sigma_{\rm tot}\rangle$ may readily be obtained [3,6].

In Ref. [45], using the results of $\sigma_{\rm tot}(\varepsilon_\nu)$ shown in the inset of Fig. 6 (bottom) for the reaction ^{130}Te$(\nu, \nu')^{130}$Te*, we estimated the supernova neutrino signal $\sigma_{\rm sign}(\varepsilon_\nu)$ on ^{130}Te by employing two-parameter Fermi-Dirac and power-law distributions (with various values of their parameters) as original supernova neutrino energy spectra (see Fig. 3 of Ref. [60]). We have also determined synthetic spectra $\eta_{\rm bb}(\varepsilon_\nu)$, defined as linear combinations of β-beam neutrino spectra with nine different Lorentz boosting factors γ, by the expression

$$\eta_{\rm bb}(\varepsilon_\nu) = \sum_{j=1}^{9} \alpha_j \sigma(\varepsilon_\nu)\eta_{\gamma_j}(\varepsilon_\nu) \tag{29}$$

and adjusting the parameters α_j by fitting them to various original supernova neutrino spectra.

We close this discussion with a concrete example of using our theoretical cross sections $\sigma(\varepsilon_\nu)$ for ^{128,130}Te isotopes in estimating neutrino fluxes, Φ_ν, or scattering event rates, $N_{\rm event}$, for the CUORE and COBRA detectors. Assuming that $N_{\rm Te}$ is the total number of nuclei (atoms) of ^{128}Te plus ^{130}Te in the detector, we have

$$\frac{dN_\nu}{dt} \equiv N_{\rm event} = N_{\rm Te}\Phi_\nu(\varepsilon_\nu)\sigma_{\rm tot}(\varepsilon_\nu)\,. \tag{30}$$

The CUORE detector is expected to have 988 crystal bolometers of TeO_2 or a total mass of ^{128}Te and ^{130}Te isotopes about $m_{\rm Te} = 392$ kg, which translates to about $N_{\rm Te} = N_{^{128}\rm Te} + N_{^{130}\rm Te} = 1.85 \times 10^{27}$ atoms (nuclei). For neutrinos of energy $\varepsilon_\nu = 50$ MeV, as can be inferred from Fig. 7, the neutral-current scattering cross section (approximately equal for both Te isotopes) is $\sigma_{\rm cum}^{\rm max}(\varepsilon_\nu = 50\ {\rm MeV}) = 3.62 \times 10^{-38}{\rm cm}^2$. For a typical detection rate of $N_{\rm event} = 1$ event hr^{-1}, the resulting from Eq. (30) neutrino flux would have to be

$$\Phi_\nu(\varepsilon_\nu = 50\ {\rm MeV}) \approx 4.1 \times 10^6\ {\rm cm}^{-2}{\rm s}^{-1}\,. \tag{31}$$

Similarly, for $\varepsilon_\nu = 30$ MeV from Fig. 7 we have $\sigma_{\rm cum}^{\rm max}(\varepsilon_\nu = 30\ {\rm MeV}) = 0.65 \times 10^{-38}$ cm^2 and the corresponding neutrino flux is

$$\Phi_\nu(\varepsilon_\nu = 30\ {\rm MeV}) \approx 2.3 \times 10^7\ {\rm cm}^{-2}\,{\rm s}^{-1}\,. \tag{32}$$

These results are encouraging for the ongoing rare event Te detectors, CUORE and COBRA, to be used in the future as astrophysical neutrino detectors in addition to their main goal of neutrinoless double-β-decay search. We should stress, however, that even though the above neutrino fluxes are of the same order with those expected at the Spallation Neutron Source at ORLaND, Oak Ridge [27,28,59], in choosing a neutrino cross section measurement target other experimental criteria usually lead to more popular choices (Xe, Cs, etc.).

A comprehensive discussion of the connection of the present study to the experiments mentioned in the Introduction through extensive convoluted cross sections calculations will be published elsewhere [61].

V. SUMMARY AND CONCLUSIONS

In view of the ongoing and expected operation of new facilities for low-energy neutrino–nucleus cross section measurements and the current activities of the extremely sensitive probes that potentially may be used for low-energy neutrino detection (MOON, COBRA, CUORE, and other experiments), reliable predictions of neutrino-scattering cross sections for various isotopes are of particular significance. In the present work, we used a microscopic approach, namely the $pp - nn$ quasiparticle RPA, to evaluate cross sections for the neutral current reactions ^{128,130}Te$(\nu, \nu')^{128,130}$Te* and ^{128,130}Te$(\widetilde{\nu}, \widetilde{\nu}')^{128,130}$Te*. The Te isotopes are main contents of the material of the COBRA and CUORE detectors with multiple neutrino physics goals (neutrinoless double-β decay and low-energy astrophysical neutrino searches). We employed the advantageous numerical method of Ref. [8] for the matrix elements of the relevant tensor multipole operators of these neutrino-nucleus processes (we do not reduce the spherical Bessel functions, coming from the Donnelly-Walecka projection functions, as is usually done, e.g., in the approximation known as long-wavelength limit).

Even though charged-current cross sections are, in general, substantially larger than the cross sections for neutral-current

scattering evaluated here, the latter may provide important information that is attributed to the following reasons. In the energy range of our calculations ($0 \leqslant \varepsilon_\nu \leqslant 100$ MeV), neutrinos are not able to produce massive (μ or τ) leptons, which means that in a low-energy neutrino detector the number of neutrinos that will participate in charged-current scattering is limited. Moreover, charged-current antineutrino scattering is suppressed for medium heavy and heavy nuclei (as is the case of ^{128,130}Te isotopes), due to Pauli blocking effects. Thus, only electron-neutrino charged-current reactions are important for such detectors, while all neutrino and antineutrino flavors take part in neutral-current scattering on, e.g., ^{128,130}Te detectors studied here, specifically heavy flavor neutrinos can be detected too.

In the present work, starting from double-differential cross sections $d^2\sigma/d\Omega d\omega$, calculated (state-by-state) with the QRPA, integrated $d\sigma/d\omega(\omega)$, total $\sigma_{\rm tot}$, and cumulative $\sigma_{\rm cum}$ ones are subsequently obtained. These cross sections may be folded with the neutrino energy distributions of specific neutrino sources to which the nuclear response is of current interest. The present results show that ^{128,130}Te present rich responses in the excitation energy range $\omega \preceq 20$ MeV (including transitions to bound states), relevant for solar neutrinos and geoneutrinos but also for the low- and intermediate-energy supernova neutrinos. These inelastic neutrino-nucleus cross sections are suitable for use in astrophysical neutrino (including supernova neutrinos) simulations utilized in order to interpret neutrino oscillations, neutrino properties, and supernova explosion mechanisms.

ACKNOWLEDGMENTS

V.T. is grateful to Prof. J.D. Vergados for fruitful discussions. Also, T.S.K. wishes to thank K. Langanke, J. Wambach, and M. Harakeh for stimulating discussions. This research was supported by the ΠΕΝΕΔ project No. 03EΔ807 of the General Secretariat for Research and Technology of the Hellenic Ministry of Development and the Helmholtz International Center for Facility for Antiproton and Ion Research (HIC for FAIR) within the framework of the LOEWE program.

APPENDIX

In our notation, the operators $\widehat{\mathcal{M}}_J$, $\widehat{\mathcal{L}}_J$, $\widehat{\mathcal{T}}^{\rm el}_J$, and $\widehat{\mathcal{T}}^{\rm mag}_J$ include polar-vector ($\hat{J}_\lambda$) and axial-vector ($\hat{J}^5_\lambda$) weak interaction pieces [1,2]. The expressions of these eight operators (that include the weak nucleon form factors) are written as

$$\hat{M}^{\rm Coul}_{JM}(q\mathbf{r}) = F_1 M^J_M(q\mathbf{r}), \tag{A1}$$

$$\hat{L}_{JM}(q\mathbf{r}) = \frac{q_0}{q}\hat{M}^{\rm Coul}_{JM}(q\mathbf{r}), \tag{A2}$$

$$\hat{T}^{\rm el}_{JM}(q\mathbf{r}) = \frac{q}{M}\left[F_1\Delta'^J_M(q\mathbf{r}) + \frac{1}{2}(F_1+2MF_2)\Sigma^J_M(q\mathbf{r})\right], \tag{A3}$$

$$i\hat{T}^{\rm mag}_{JM}(q\mathbf{r}) = \frac{q}{M}\left[F_1\Delta^J_M(q\mathbf{r}) - \frac{1}{2}(F_1+2MF_2)\Sigma'^J_M(q\mathbf{r})\right], \tag{A4}$$

$$i\hat{M}^5_{JM}(q\mathbf{r}) = \frac{q}{M}\left[F_A\Omega^J_M(q\mathbf{r}) + \frac{1}{2}(F_A+q_0F_P)\Sigma''^J_M(q\mathbf{r})\right], \tag{A5}$$

$$-i\hat{L}^5_{JM}(q\mathbf{r}) = \left[F_A - \frac{q^2}{2M}F_P\right]\Sigma''^J_M(q\mathbf{r}), \tag{A6}$$

$$-i\hat{T}^{\rm el5}_{JM}(q\mathbf{r}) = F_A\Sigma'^J_M(q\mathbf{r}), \tag{A7}$$

$$\hat{T}^{\rm mag5}_{JM}(q\mathbf{r}) = F_A\Sigma^J_M(q\mathbf{r}). \tag{A8}$$

The pseudoscalar form factor F_P is usually neglected (see Sec. III). The multipole operators of Eqs. (A1)–(A3) and (A8) are of normal parity, $\pi = (-)^J$, while the others have abnormal parity, $\pi = (-)^{J+1}$.

The seven new operators, $M^{\rm Coul}_{JM}$, Δ^J_M, Δ'^J_M, Ω^J_M, Σ^J_M, Σ'^J_M, and Σ''^J_M, which appear on the right-hand side of Eqs. (A1)–(A8) (due to CVC theory), are linearly independent. Their reduced matrix elements, which are of the form $\langle j_1||T^J_i||j_2\rangle$ where T^J_i represent any of these basic tensor multipole operators, have been written in closed compact formulas [8] as

$$\langle j_1\|T^J\|j_2\rangle = e^{-y}y^{\beta/2}\sum_{\mu=0}^{n_{\rm max}}\mathcal{P}^J_\mu\, y^\mu, \tag{A9}$$

where the geometrical coefficients $\mathcal{P}^J_\mu$ are rational numbers or square roots of rational numbers throughout the model space (proton neutron configurations) and may be calculated once at the beginning of our calculations.

In the latter summation the upper index $N_{\rm max}$ represents the maximum harmonic oscillator quanta included in the model space chosen,

$$n_{\rm max} = (N_1 + N_2 - \beta)/2, \tag{A10}$$

where $N_\lambda = 2n_\lambda + \ell_\lambda$ and $j_\lambda \equiv (n_\lambda, \ell_\lambda)j_\lambda$ and β is related to the rank of the above operators (see Ref. [8]).

[1] T. W. Donnelly and J. D. Walecka, Nucl. Phys. A **274**, 368 (1976).
[2] T. W. Donnelly and R. D. Peccei, Phys. Rep. **50**, 1 (1979).
[3] E. Kolbe and T. S. Kosmas, Springer Tracts Mod. Phys. **163**, 199 (2000).
[4] H. Ejiri, Phys. Rep. **338**, 265 (2000).
[5] J. D. Vergados, Phys. Rep. **361**, 1 (2002).
[6] T. S. Kosmas and E. Oset, Phys. Rev. C **53**, 1409 (1996).
[7] E. Kolbe, Phys. Rev. C **54**, 1741 (1996).
[8] V. Ch. Chasioti and T. S. Kosmas, Nucl. Phys. A **829**, 234 (2009).
[9] K. Langanke, Acta Phys. Pol. B **39**, 265 (2008).
[10] H.-Th. Janka, K. Langanke, A. Marek, G. Martinez-Pinedo, and B. Mueller, Phys. Rep. **442**, 38 (2007).
[11] Y. Giomataris and J. D. Vergados, Phys. Lett. B **634**, 23 (2006).
[12] J. D. Vergados and Y. Giomataris, Phys. At. Nucl. **70**, 140 (2007).
[13] J. W. F. Valle, J. Phys. Conf. Ser. **203**, 012009 (2010); arXiv:1001.5189 [hep-ph] (2010).

[14] J. D. Vergados, F. T. Avignone, and I. Giomataris, Phys. Rev. D **79**, 113001 (2009).
[15] E. Kolbe, K. Langanke, G. Martinez-Pinedo, and P. Vogel, J. Phys. G **29**, 2569 (2003).
[16] C. Froehlich, G. Martinez-Pinedo, M. Liebendoerfer, F.-K. Thielemann, E. Bravo, W. R. Hix, K. Langanke, and N. T. Zinner, Phys. Rev. Lett. **96**, 142502 (2006).
[17] K. Zuber, Prog. Part. Nucl. Phys. **57**, 235 (2006).
[18] K. Zuber, Phys. Lett. B **519**, 1 (2001); private communication (2007).
[19] H. Ejiri, J. Engel, R. Hazama, P. Krastev, N. Kudomi, and R. G. H. Robertson, Phys. Rev. Lett. **85**, 2917 (2000).
[20] C. Arnaboldi *et al.*, Phys. Rev. C **78**, 035502 (2008).
[21] M. N. Harakeh and A. van der Woude, *Giant Resonances* (Clarendon, Oxford, 2001); private communication (2010).
[22] P. Zucchelli, Phys. Lett. B **532**, 166 (2002).
[23] C. Volpe, J. Phys. G **30**, L1 (2004).
[24] C. Volpe, J. Phys. G **34**, R1 (2007).
[25] N. Jachowicz, K. Vantournhout, J. Ryckebusch, and K. Heyde, Phys. Rev. Lett. **93**, 082501 (2004).
[26] W. C. Louis, Prog. Part. Nucl. Phys. D **63**, 51 (2009).
[27] F. T. Avignone and Y. V. Efremenko, Nucl. Phys. B, Proc. Suppl. **87**, 304 (2000).
[28] F. T. Avignone and Y. V. Efremenko, J. Phys. G **29**, 2615 (2003).
[29] R. L. Burman and W. C. Louis, J. Phys. G **29**, 2499 (2003).
[30] C. Volpe, N. Auerbach, G. Coló, T. Suzuki, and N. Van Giai, Phys. Rev. C **62**, 015501 (2000).
[31] T. S. Kosmas, Nucl. Phys. A **683**, 443 (2001).
[32] T. W. Donnelly and J. D. Walecka, Phys. Lett. B **41**, 275 (1972).
[33] T. W. Donnelly and J. D. Walecka, Nucl. Phys. A **201**, 81 (1973).
[34] W. C. Haxton, Phys. Rev. D **36**, 2283 (1987).
[35] S. W. Bruenn and W. C. Haxton, Astrophys. J. **376**, 678 (1991).
[36] V. Ch. Chasioti, T. S. Kosmas, and P. C. Divari, Prog. Part. Nucl. Phys. **59**, 481 (2007).
[37] M. S. Athar and S. K. Singh, Phys. Lett. B **591**, 69 (2004).
[38] M. S. Athar, S. Ahmad, and S. K. Singh, Phys. Rev. C **71**, 045501 (2005).
[39] T. S. Kosmas, J. D. Vergados, O. Civitarese, and A. Faessler, Nucl. Phys. A **570**, 637 (1994).
[40] T. S. Kosmas, A. Faessler, F. Simkovic, and J. D. Vergados, Phys. Rev. C **56**, 526 (1997).
[41] V. A. Rodin, A. Faessler, F. Simkovic, and P. Vogel, Nucl. Phys. A **766**, 107 (2006).
[42] A. Faessler, Nucl. Phys. B, Proc. Suppl. **188**, 20 (2009).
[43] P. Ring and P. Schuck, *The Nuclear Many-Body Problem* (Springer, Berlin, 1980).
[44] N. Jachowicz, K. Heyde, and J. Ryckebusch, Phys. Rev. C **66**, 055501 (2002).
[45] V. Tsakstara, T. S. Kosmas, and J. Sinatkas, Prog. Part. Nucl. Phys. **66**, 430 (2011).
[46] V. Tsakstara, Ph.D. thesis, Ioannina University Press, 2010.
[47] N. Jachowicz, S. Rombouts, K. Heyde, and J. Ryckebusch, Phys. Rev. C **59**, 3246 (1999).
[48] E. Kolbe and K. Langanke, Phys. Rev. C **63**, 025802 (2001).
[49] J. Toivanen, E. Kolbe, K. Langanke, G. Martinez-Pinedo, and P. Vogel, Nucl. Phys. A **694**, 395 (2001).
[50] E. Kolbe, K. Langanke, and P. Vogel, Phys. Rev. D **66**, 013007 (2002).
[51] V. Tsakstara, T. S. Kosmas, P. C. Divari, and J. Sinatkas, Prog. Part. Nucl. Phys. **64**, 411 (2010).
[52] J. Schwieger, T. S. Kosmas, and A. Faessler, Phys. Rev. C **56**, 2830 (1997).
[53] P. Papakonstantinou, T. S. Kosmas, J. Wambach, and A. Faessler, Phys. Rev. C **73**, 035502 (2006).
[54] P. Papakonstantinou, O. Civitarese, T. S. Kosmas, and J. Wambach, Czech. J. Phys. **56**, 481 (2006).
[55] V. Tsakstara, T. S. Kosmas, and P. C. Divari, J. Phys. Conf. Ser. **203**, 012093 (2010); V. Tsakstara and T. S. Kosmas, Prog. Part. Nucl. Phys. **64**, 407 (2010).
[56] E. V. Bugaev, G. S. Bisnovatyi-Kogan, M. A. Rudzsky, and Z. F. Seidov, Nucl. Phys. A **324**, 350 (1979).
[57] P. Divari and T. S. Kosmas, HNPS: Advances in Nuclear Physics, Proc. 17th Hellenic Symposium 75 (2008).
[58] The Borexino Collaboration, arXiv:hep-ex/1104.1816v1 (2011).
[59] J. D. Vergados, arXiv:1103.1107v1 [hep-ph] (2011).
[60] V. Tsakstara, T. S. Kosmas, and J. Wambach, Prog. Part. Nucl. Phys. **66**, 424 (2011).
[61] V. Tsakstara and T. S. Kosmas (unpublished).